





## Article

# Outage Probability Analysis in Relaying Cooperative Systems with NOMA Considering Power Splitting

Tran Thai Hoc Ly <sup>1,2</sup>, Hoang-Sy Nguyen <sup>1,3</sup>, Thanh-Sang Nguyen <sup>1</sup>, Van Van Huynh <sup>4,\*</sup>,  
Thanh-Long Nguyen <sup>1,5</sup> and Miroslav Voznak <sup>1</sup>

<sup>1</sup> Dept. of Telecommunications, VSB-Technical University of Ostrava, 17. listopadu 15/2172, 708 33 Ostrava-Poruba, Czech Republic; ntsang@bdu.edu.vn (T.-S.N.); miroslav.voznak@vsb.cz (M.V.)

<sup>2</sup> Nguyen Tat Thanh University, Ho Chi Minh City, Vietnam; ltthoc@ntt.edu.vn

<sup>3</sup> Institute of Artificial Intelligence, Binh Duong University, Thu Dau Mot City, Binh Duong Province, Vietnam; nhsy@bdu.edu.vn

<sup>4</sup> Modeling Evolutionary Algorithms Simulation and Artificial Intelligence, Faculty of Electrical & Electronics Engineering, Ton Duc Thang University, Ho Chi Minh City, Vietnam

<sup>5</sup> Center for Information Technology, Ho Chi Minh City University of Food Industry, Ho Chi Minh City, Vietnam; longthng@gmail.com

\* Correspondence: huynhvanvan@tdtu.edu.vn; Tel.: +84-283-775-5028

Received: 16 December 2018; Accepted: 7 January 2019; Published: 10 January 2019



**Abstract:** In recent years, non-orthogonal multiple access (NOMA) has become a promising technology for the advancement of future wireless communications. In principle, the relay node with better channel conditions can support others to enhance the system performance by using successive interference cancellation (SIC) technique. In this paper, we take advantage of NOMA in the study of a relaying cooperative system operating in half-duplex (HD) fixed decode-and-forward (DF) relaying scheme. In the two time slots, two data symbols are received at the destination node resulting in a higher transmission rate. Besides that, we study energy harvesting (EH) with power splitting (PS) protocol. For performance analysis, approximate and exact closed-form expressions for outage probability (OP) are obtained. Following that, we examine the average bit error probability (ABEP) while expressions for the throughput in delay-limited mode are given. It can be seen that our simulation results match well with the Monte Carlo simulations.

**Keywords:** NOMA; energy harvesting; power splitting; bit error probability; outage probability

## 1. Introduction

In order to meet the demand for high energy consumption in future wireless communications, energy harvesting (EH) from radio frequency (RF) has increasingly become a promising technology, in which energy received from RF signals is converted into electricity to power wireless devices. Thanks to this technology, both energy and information can be simultaneously transmitted to wireless users located near the source node [1–6]. In fact, EH and information transmission (IT) cannot be carried out at the same time. Thus, the received signal has to be divided for EH and IT by either two foundational receiver architectures, i.e., or time switching (TS) and power splitting (PS) [7,8]. In particular, the literature in [9] developed two optimal TS policies, namely Optimal Time for Transmit Power at Source and Optimal Time for Transmit Power at Relay when considering a half-duplex (HD) decode-and-forward (DF) small cell cognitive relay network (CRN).

Besides, an EH relaying network was evaluated in terms of the outage probability (OP) in [10], in which closed-form expressions for OP over Nakagami-m fading channels for both amplify-and-forward (AF) and DF relaying schemes were obtained. Interestingly, it is worth noting

that PS protocol is proved to be better than TS although PS is complicated and inefficient for practical implementations. Nevertheless, there have been several investigations into the use of PS [11–13]. In [11], the authors focused on PS scheme in an AF system, in which an optimization issue was solved to minimize the impact of instantaneous channel state information (CSI), in which the PS ratio is able to adjust itself according to the instantaneous CSI. Similarly, the PS ratio can be changed based on CSI in [12]. In addition, the work in [13] addressed the trade-off between the achievable information rate and the harvested energy for a PS receiver architecture. In [14], a dynamic PS scheme was studied in which trade-offs between the maximum ergodic capacity for IT and the maximum average harvested energy for power transfer. Furthermore, the study in [15] considered PS protocol, in which the authors tried to optimize their PS ratios and the transmit power to maximize the data rate over multiple coherent time slots. In [16], different two-way relay networks were considered, in which the performance of these considered systems were examined based on PS and TS protocols. In addition, the literature in [17] focused on a symmetric wireless communication network with SWIPT in a K-user multiple-input multiple-output (MIMO) CRN, where PS ratio and power allocation were carefully investigated to guarantee the ideal system performance.

In recent years, non-orthogonal multiple access (NOMA) has increasingly become a potential multiple access technology in order to enhance the spectral efficiency (SE) of mobile systems [18]. For instance, multiuser superposition transmission was proposed for Third Generation Partnership Project LTE-Advanced (3GPP-LTE-A) networks as a downlink version of NOMA. Besides that, NOMA has caught much research interest as a key technique in future 5G mobile networks.

Unlike previous wireless networks which depend on the time, frequency, and code domain, NOMA takes advantage of the power domain for multiple access. For example, the primary problem with frequency-division multiple access deployed by 3GPP-LTE is the low SE if some bandwidth resources like subcarrier channels are allocated to users with poor channel conditions [19]. Meanwhile, NOMA technique allows access to all the subcarrier channels, so users with strong channel conditions are able to access bandwidth resources allocated to users with poor channel conditions. This nature results in better SE [20]. In addition, NOMA balances the user fairness and the system throughput while conventional orthogonal multiple access (OMA) only serves users with strong channel conditions [21]. This is because users with different channel conditions can be served timely which meets the rising demands for ultra-low latency and ultra-high connectivity in 5G future communications.

In EH-based NOMA systems, there have been a number of investigations conducted on different sorts of systems, i.e., cooperative relaying networks (CRNs), wireless sensor networks (WSNs), and cognitive relaying (CNs) [22–27]. In [22], EH CRN NOMA system was studied, in which three different relaying protocols AF, DF, and quantize-map-forward (QF) were taken into comparisons. Besides that, the outage probability (OP) of the EH NOMA relaying network was examined in [23], where the transmitting antenna selection is applied at BS and maximal ratio combining is applied at the multiple users. The literature in [24] focused on three different cognitive NOMA architectures, including underlay NOMA networks, overlay NOMA networks, and CR-inspired NOMA networks. In addition, the authors in [25] considered the interference from different sources at the sensors in WSNs. After achieving the expressions for OP, they examined the average link throughput and energy consumption efficiency of NOMA against conventional OMA technique. Likewise, [26] considered a WSN, an energy efficiency (EE) optimization problem was proposed which challenging difficult to solve for global optimality due to the lack of convexity. In [27], the authors examined the bit error rate (BER) and the performance capacity of a typical NOMA system.

Motivated from those aforementioned works, we try to derive approximate and exact closed-form expressions for OP. Besides, we study the average bit error probability (ABEP) together with the delay-limited throughput to fully understand the benefits of NOMA, and we realize that the system performance is better than traditional relaying systems in the case of deploying NOMA.

We divide this work into five sections. In particular, Section 2 provides the system model. The system performance analysis is done in Section 3, where expressions for OP, ABEP, and the

delay-limited throughput are obtained. We prove the system performance by giving some numerical results in Section 4. Finally, a brief conclusion is given in Section 5.

**Notation:** We present the cumulative distribution function (CDF) and probability density function (PDF) of the random variable (RV) as  $F_X(a) = 1 - \frac{1}{\Omega_h} e^{-\frac{a}{\Omega_h}}$  and  $f_X(a) = \frac{1}{\Omega_h} e^{-\frac{a}{\Omega_h}}$ , where  $\Omega_a$  is the average power.  $Pr(\cdot)$  stands for the probability distribution.  $\mathbb{E}\{|\cdot|\}$  is the expectation operator. Besides that,  $K_1(\cdot)$  stands for the modified Bessel function of the second kind with order 1. The Whittaker function is  $W_{\mu,\nu}(\cdot)$ .

## 2. System Model

We considered a cooperative relaying non-orthogonal multiple access (CR-NOMA) system depicted Figure 1. Particularly, a source node (S), a relay node, and a destination node (D) communicate with each other, but R is used to support the communication between S and D because of the far distance. In this model, we assume R operates in decode-and-forward (DF) half-duplex (HD) relaying mode. It is worth noting that the direct transmission is also possible. In addition, the additive white Gaussian noise (AWGN) has an impact on all nodes' received signals with zero mean  $n_0$  and variance  $N_0$ . In this work,  $d_{SR}$  and  $d_{RD}$  are used to denote the distances between S-R and R-D links, respectively.

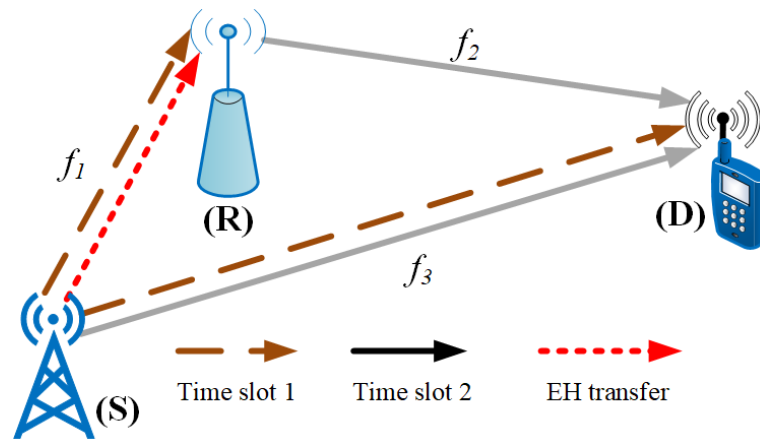
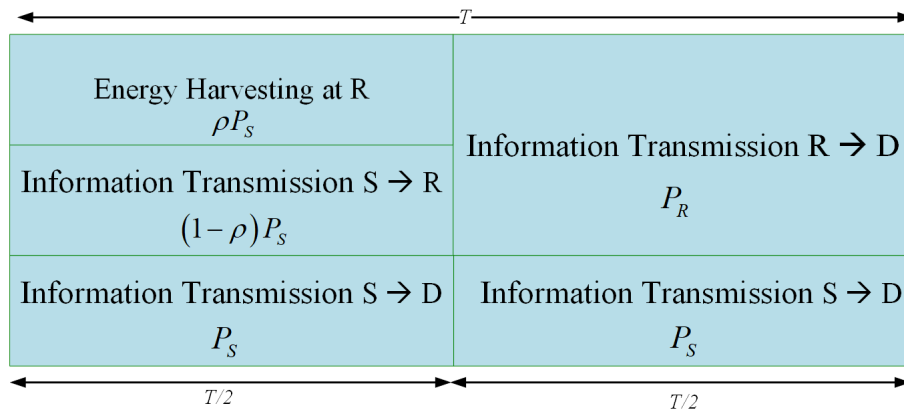


Figure 1. System model.

In principle, there are two time slots involved in each system communication process. Regarding the first time slot, S transfers a signal symbol denoted as  $x_1$  with the transmit power  $P_S$  to R and D, where  $\mathbb{E}(|x_1|^2) = 1$ . Interestingly, thanks to the different receiver mechanisms, two signals are split and differentiated with the power allocation at S as in [21]. Following that, another signal symbol denoted as  $x_2$  is transferred to D with  $P_S$  in the second time slot, in which  $\mathbb{E}(|x_2|^2) = 1$ . It is noted that D simultaneously receives  $x_1$  from R with the transmit power,  $P_R$  in the second time slot.

Regarding the system channels, we represent the channel coefficients of S-R, R-D, and S-D links as  $f_1$ ,  $f_2$ , and  $f_3$ , and they are affected by independent and identically distributed (i.i.d) quasi-static Rayleigh fading channel. In addition, the channel power gain is denoted by  $|A|^2$  with  $A \in \{f_1, f_2, f_3\}$  following an exponential distribution with the mean value,  $\Omega_A$ .

In order to examine energy harvesting (EH) in this model, we decided to deploy power spitting (PS) protocol showed Figure 2. In particular, the block time,  $T$  is divided for each transmission slot. In principle, the PS ratio,  $\rho P_S$  splits a part of the received signal power with  $0 \leq \rho \leq 1$  divided for EH while the remaining part,  $(1 - \rho)P_S$  used for information transmission (IT).



**Figure 2.** Energy harvesting and information transmission protocol.

Therefore, we express the received signal at  $R$  in the first time slot as

$$\sqrt{\rho} y_{R,1,x_1} = \sqrt{\frac{\rho P_S}{d_{SR}^m}} f_1 x_1 + n_0, \quad (1)$$

where the path-loss exponent is  $m$ .

Following from (1), the harvested energy at  $R$  is calculated as

$$E_h = \frac{T}{2} \eta \rho P_S d_{SR}^{-m} |f_1|^2, \quad (2)$$

where the energy conversion efficiency is defined as  $0 \leq \eta \leq 1$  relying on the EH circuitry and rectification.

The transmit power at  $R$  is calculated with a small portion of the energy stored at itself. In particular,  $w$  and  $wP_S$  are used to represent the fractional constant and the transmit power supplied by the battery, respectively. We assume when  $w = 0$ , the transmit power at  $R$  is solely provided by the energy harvested from  $S$ . Hence, we can express the transmit power at  $R$  within  $T/2$  as

$$P_R = \frac{2E_h}{T} + wP_S = \eta \rho P_S d_{SR}^{-m} |f_1|^2. \quad (3)$$

However, the signal  $x_1$  received at  $R$  is expressed by

$$\sqrt{1 - \rho} y_{R,1,x_1} = \sqrt{\frac{(1 - \rho) P_S}{d_{SR}^m}} f_1 x_1 + n_0. \quad (4)$$

In addition, the same applies for  $D$  as

$$y_{D,1,x_1} = \sqrt{\frac{P_S}{d_{SD}^m}} f_3 x_1 + n_0, \quad (5)$$

where  $d_{SD}$  is denoted the distance between  $S$  and  $D$  link.

We define the received signal-to-noise ratio (SNR) as  $\gamma = \mathbb{E} \{ |\text{signal}|^2 \} / \mathbb{E} \{ |\text{overall noise}|^2 \}$ . Thus, following from (4) and (5), the SNRs for  $x_1$  at both  $R$  and  $D$  can be respectively obtained as

$$\gamma_{R,1,x_1} = \frac{\beta(1 - \rho) |f_1|^2}{d_{SR}^m}, \quad (6a)$$

and

$$\gamma_{D,1,x_1} = \frac{\beta |f_3|^2}{d_{SD}^m}, \quad (6b)$$

where the transmit SNR is written as  $\beta = P_S / N_0$ .

In this system model,  $D$  receives signals from  $S$  while using successive interference cancellation (SIC) to conduct successful signal decoding. Therefore, we compute the received signal at  $D$  as

$$y_{D,2} = \sqrt{\frac{P_R}{d_{RD}^m}} f_2 x_1 + \sqrt{\frac{P_S}{d_{SD}^m}} f_3 x_2 + n_0. \quad (7)$$

Replacing (3) into (7), we can rewrite (7) as

$$y_{D,2} = \sqrt{\frac{\eta \rho P_S |f_1|^2}{d_{SR}^m d_{RD}^m}} f_2 x_1 + \sqrt{\frac{P_S}{d_{SD}^m}} f_3 x_2 + n_0. \quad (8)$$

In fact, due to the different locations wireless nodes, the fading gain of the  $R$ - $D$  channel,  $f_2$  is proved to be more significant than that of the  $S$ - $D$  channel,  $f_3$ . Due to the natural characteristics of different transceivers' channels, it motivates us to apply NOMA in the second time slot. Thanks to the deployment of SIC,  $D$  treats  $x_1$  while considering  $x_2$  as a noise term. As a consequence, we have to remove  $x_1$  from  $y_{D,2}$  to successfully decode  $x_2$ . Hence, the received SNRs at  $D$  for both data symbols can be obtained as

$$\gamma_{D,2,x_1} = \frac{\frac{\eta \rho \beta}{d_{SR}^m d_{RD}^m} |f_1|^2 |f_2|^2}{\frac{\beta}{d_{SD}^m} |f_3|^2 + 1}, \quad (9a)$$

and

$$\gamma_{D,2,x_2} = \frac{\beta |f_3|^2}{d_{SD}^m}. \quad (9b)$$

Thanks to the use of R, the end-to-end SNR for  $x_1$  can be obtained as

$$\gamma_{e2e,x_1} = \min \{ \gamma_{R,1,x_1}, \gamma_{D,2,x_1} \}. \quad (10)$$

The data rate the end-to-end SNR at  $D$  for  $x_1$  and both  $x_1$  and  $x_2$  can be written with fixed DF relaying scheme as

$$R_{e2e,x_1} = \frac{1}{2} \log_2 (1 + \gamma_{e2e,x_1}), \quad (11a)$$

and

$$R_{D,1,x_1} = R_{D,2,x_2} = \frac{1}{2} \log_2 (1 + \gamma_{D,1,x_1}), \quad (11b)$$

where we defined  $\gamma_{e2e,x_1}, \gamma_{D,1,x_1}$  above.

### 3. Performance Analysis

In this section, we are going to provide exact and approximate closed-form expressions for outage probability ( $OP$ ). Besides that, the average bit error probability (ABEP) and delay-limited throughput are going to be examined to comprehensively study CR-NOMA. Let us start first with the study of  $OP$ .

#### 3.1. Exact Outage Performance

In principle, the  $OP$  denoted as  $OP$  represents the probability in which the instantaneous SNR,  $\gamma$  is set below its own threshold defined as  $\gamma_0$ . In this paper, we define  $OP$  as  $OP = \Pr(\gamma < \gamma_0) = F_\gamma(\gamma_0)$ .

Let us first investigate the CDF in Proposition 1.

**Proposition 1.** *OPs for  $x_1$  and  $x_2$  presented as  $OP_{x_1}$  and  $OP_{x_2}$  can be computed as*

$$OP_{x_1} = (1 - e^{-v_1}) \times \left( 1 - \frac{1}{\Omega_{f_3}} \int_{x=0}^{\infty} e^{-\frac{x}{\Omega_{f_3}} - v_2} \mu_1 K_1(\mu_1) dx \right), \quad (12)$$

and

$$OP_{x_2} = 1 - \frac{1}{\Omega_{f_3}} e^{-v_1} \int_{x=0}^{\infty} e^{-\frac{x}{\Omega_{f_3}}} \mu_1 K_1(\mu_1) dx, \quad (13)$$

where  $v_1 = \frac{d_{SD}^m \gamma_0}{\beta \Omega_{f_3}}$ ,  $v_2 = \frac{d_{SR}^m \gamma_0}{\beta(1-\rho)\Omega_{f_1}}$  and  $\mu_1 = \sqrt{\frac{4d_{SR}^m d_{RD}^m \gamma_0}{\eta \rho \beta \Omega_{f_1} \Omega_{f_2}} \left( \frac{\beta}{d_{SD}^m} x + 1 \right)}$ .

**Proof.** Thanks to the CDF for  $\gamma_{R,1,x_1}$  and  $\gamma_{D,1,x_1}$ , we achieve

$$F_{\gamma_{R,1,x_1}}(\gamma_0) = 1 - e^{-\frac{d_{SR}^m \gamma_0}{\beta(1-\rho)\Omega_{f_1}}}, \quad (14a)$$

and

$$F_{\gamma_{D,1,x_1}}(\gamma_0) = 1 - e^{-\frac{d_{SD}^m \gamma_0}{\beta \Omega_{f_3}}}. \quad (14b)$$

To obtain the OP for  $x_1$  at D, the CDF of  $\gamma_{D,2,x_1}$  must be achieved first. Thus, we condition  $F_{\gamma_{D,2,x_1}}(\gamma_0)$  on  $|f_3|^2$  as follows

$$\begin{aligned} F_{\gamma_{D,2,x_1}}(\gamma_0) &= \Pr \left( |f_1|^2 \leq \frac{\gamma_0 d_{SR}^m d_{RD}^m \left( \frac{\beta |f_3|^2}{d_{SD}^m} + 1 \right)}{\eta \rho \beta |f_2|^2} \right) \\ &= \frac{1}{\Omega_{f_2}} \int_{x=0}^{\infty} \left( 1 - e^{-\frac{1}{x} \left( \frac{\gamma_0 d_{SR}^m d_{RD}^m \left( \frac{\beta |f_3|^2}{d_{SD}^m} + 1 \right)}{\eta \rho \beta \Omega_{f_1}} \right)} \right) e^{-\frac{x}{\Omega_{f_2}}} dx. \end{aligned} \quad (15)$$

By taking advantage of ([28], Equation (3.324.1)), we have

$$\int_0^{\infty} e^{-\frac{\beta}{4x} - \eta \rho x} dx = \sqrt{\frac{\beta}{\eta \rho}} K_1(\sqrt{\beta \eta \rho}). \quad (16)$$

Thus, the CDF of  $\gamma_{D,2,x_1}$  over  $|f_3|^2$  can be expressed by

$$F_{\gamma_{D,2,x_1}}(\gamma_0) = 1 - \frac{1}{\Omega_{f_3}} \int_0^{\infty} \left( e^{-\frac{x}{\Omega_{f_3}} - v_2} \mu_1 K_1(\mu_1) \right) dx. \quad (17)$$

If  $x_1$  is not decoded, outage events may occur. Therefore, applying (14a) and (17), the OP at the end-to-end SNR at D is written by

$$\begin{aligned} OP_{e2e,x_1} &\triangleq F_{\gamma_{R,1,x_1}}(\gamma_0) + F_{\gamma_{D,2,x_1}}(\gamma_0) - F_{\gamma_{R,1,x_1}}(\gamma_0) F_{\gamma_{D,2,x_1}}(\gamma_0) \\ &\triangleq 1 - \frac{1}{\Omega_{f_3}} \int_{x=0}^{\infty} \left( e^{-\frac{x}{\Omega_{f_3}} - \frac{d_{SR}^m \gamma_0}{\beta(1-\rho)\Omega_{f_1}}} \mu_1 K_1(\mu_1) \right) dx. \end{aligned} \quad (18)$$

Thanks to selection combining technique, the total value of OP,  $x_1$  can be computed as

$$OP_{x_1} = F_{\gamma_{D,1,x_1}}(\gamma_0) \times OP_{e2e,x_1}. \quad (19)$$

Substituting (14b) and (18) into (19), (12) was derived. In addition, the OP of  $x_2$  is expressed as

$$OP_{x_2} = 1 - \left(1 - F_{\gamma_{D,2,x_1}}(\gamma_0)\right) \times \left(1 - F_{\gamma_{D,2,x_2}}(\gamma_0)\right), \quad (20)$$

where  $F_{\gamma_{D,2,x_2}}$  is presented in (14b).

This ends the proof for Proposition 1.  $\square$

**Remark 1.** *OP varies as a function of PS ratio,  $\rho$  ranging from 0 to 1. It is noted that the more  $\rho$  is, the more transmit power is available at R. As a result, if there is more transmit power at R, fewer outage events are likely to occur.*

### 3.2. Approximate Outage Performance

Due to the involvement of an integral in the above expression for OP which is not closed-form in Proposition 1, the asymptotic OP expressions at high SNR regime in Proposition 2 are going to be expressed as the following tight upper bound function.

**Proposition 2.** *At high SNR regime, we can express the approximate expressions for OP with  $a$  and  $b$  standing for the communication via R and the direct transmission as*

$$OP_{(\beta \rightarrow \infty)}^{(x_1)} \approx v_1 - v_1(1 - v_2)e^{\frac{1}{2}\mu_2}W_{-1, \frac{1}{2}}(\mu_2), \quad (21)$$

and

$$OP_{(\beta \rightarrow \infty)}^{(x_2)} \approx 1 - (1 - v_1)e^{\frac{1}{2}\mu_2}W_{-1, \frac{1}{2}}(\mu_2), \quad (22)$$

where  $\mu_2 = \frac{d_{SR}^m d_{RD}^m d_{SD}^{-m} \Omega_{f_3} \gamma_0}{\eta \rho \Omega_{f_1} \Omega_{f_2}}$ .

**Proof.** Similar to steps conducted in the proof for Proposition 1, the modified Bessel function of the second kind as,  $xK_1(x) \rightarrow 1$  can be upper bounded when  $x \rightarrow 0$ . Therefore, at high SNR, the CDF in (17) with  $\beta \rightarrow \infty$  can be expressed again as

$$\begin{aligned} F_{\gamma_{D,2,x_1}}(\gamma_0) &= 1 - \frac{1}{\Omega_{f_3}} \int_0^\infty \left( e^{-\frac{x}{\Omega_{f_3}}} \mu_1 K_1(\mu_1) \right) dx \\ &\leq 1 - \frac{2}{\Omega_{f_3}} \sqrt{\frac{d_{SR}^m d_{RD}^m d_{SD}^{-m} \Omega_{f_3} \gamma_0}{\eta \rho \Omega_{f_1} \Omega_{f_2}}} \int_{x=0}^\infty e^{-\frac{x}{\Omega_{f_3}}} \sqrt{x} K_1 \left( 2 \sqrt{\frac{d_{SR}^m d_{RD}^m d_{SD}^{-m} \Omega_{f_3} \gamma_0}{\eta \rho \Omega_{f_1} \Omega_{f_2}}} \sqrt{x} \right) dx. \end{aligned} \quad (23)$$

Thanks to the integral identity in ([28], Equation (6.643.2)), we have

$$\int_0^\infty x^{\mu-\frac{1}{2}} e^{-\alpha x} K_{2\nu}(2\beta\sqrt{x}) dx = \frac{\Gamma\left(\mu + \nu + \frac{1}{2}\right) \Gamma\left(\mu - \nu + \frac{1}{2}\right)}{2\beta} e^{\frac{\beta^2}{2\alpha}} \alpha^{-\mu} W_{-\mu, \nu} \left( \frac{\beta^2}{\alpha} \right), \quad (24)$$

Following that, we derive

$$F_{\gamma_{B,2,TS}}^{(x_1)}(\gamma_0) \leq 1 - e^{\frac{1}{2} \frac{d_{SR}^m d_{RD}^m d_{SD}^{-m} \Omega_{f_3} \gamma_0}{\eta \rho \Omega_{f_1} \Omega_{f_2}}} W_{-1, \frac{1}{2}} \left( \frac{d_{SR}^m d_{RD}^m d_{SD}^{-m} \Omega_{f_3} \gamma_0}{\eta \rho \Omega_{f_1} \Omega_{f_2}} \right). \quad (25)$$

To this point,  $e^{-x} = 1 - x$  can be approximated when  $x \rightarrow 0$  as in ([28], Equation (1.211.1)) from (12). After some algebraic manipulations, (21) and (22) are obtained for the proof of Proposition 2.  $\square$

### 3.3. Average Bit Error Probability (ABEP)

In principle, the average bit error probability (ABEP) is known as the probability used to examine the performance of wireless applications. Considering various modulations, i.e., BPSK, BFSK with



orthogonal signaling, and  $M$ -ary square QAM alphabet, which transmits data by changing the amplitude of two carrier signals.

For the sake of simplicity, the ABEP,  $P_b(e)$  for the end-to-end SNR,  $\gamma_{e2e}$  can be expressed by

$$P_b = \int_{\gamma=0}^{\infty} P_b(e|\gamma) f_{e2e}(\gamma) d\gamma, \quad (26)$$

where  $P_b(e|\gamma)$  is averaging the conditional BEP over the PDF.

Using BEP in an AWGN channel [29], the  $k$ -th bit ABEP of Gray bit-mapped  $M$ -ary square QAM is given by

$$P_b(e|k) = \frac{2}{\sqrt{M}} \sum_{i=0}^{(1-2^{-k})\sqrt{M}-1} \left\{ (-1)^{\left\lfloor \frac{i2^{k-1}}{\sqrt{M}} \right\rfloor} \left( 2^{k-1} - \left\lfloor \frac{i2^{k-1}}{\sqrt{M}} + \frac{1}{2} \right\rfloor \right) \times \varepsilon \left[ Q(2i+1) \sqrt{\frac{3\gamma}{M-1}} \right] \right\}, \quad (27)$$

where  $\varepsilon[\cdot]$  denotes the statistical expectation operator, and  $Q(x)$  is the Gaussian Q-function defined as  $Q(x) = \frac{1}{\sqrt{2\pi}} \int_x^{\infty} e^{-t^2/2} dt$ , and  $x \leq 0$ .

Eventually, the ABEP of  $M$ -ary square QAM can be written as

$$P_b(e) = \frac{1}{\log_2 \sqrt{M}} \sum_{k=0}^{\log_2 \sqrt{M}} P_b(e|k). \quad (28)$$

In order to compute the ABEP as in [29], the following expression is given

$$\mathcal{B} = E \left[ pQ \left( \sqrt{2q\gamma} \right) \right], \quad (29)$$

where  $(p, q) = (1, 2)$  for BPSK, and  $(p, q) = (1, 1)$  for QPSK. Consequently, before obtaining the ABEP, the distribution function of  $\gamma$  must be expected.

Then, the expression for ABEP derived in (29) is rewritten over the CDF as

$$\mathcal{B} = \frac{p\sqrt{q}}{2\sqrt{\pi}} \int_{\gamma=0}^{\infty} \frac{e^{-q\gamma}}{\sqrt{\gamma}} F_{\gamma_{e2e}}(\gamma) d\gamma. \quad (30)$$

The total ABEP of  $x_1$  is given by

$$\mathcal{B}_{sum, x_1} = \frac{p\sqrt{q}}{2\sqrt{\pi}} \int_{\gamma=0}^{\infty} \frac{e^{-q\gamma}}{\sqrt{\gamma}} \left( F_{\gamma_{D,1,x_1}}(\gamma) + F_{\gamma_{e2e,x_1}}(\gamma) \right) d\gamma, \quad (31)$$

where  $F_{\gamma_{D,1,x_1}}, F_{\gamma_{e2e,x_1}}$  are respectively presented in (14b) and (18).

Likewise, the ABEP of  $x_2$  can be derived based on (30) as  $\mathcal{B}_{x_2} = \frac{p\sqrt{q}}{2\sqrt{\pi}} \int_{\gamma=0}^{\infty} \frac{e^{-q\gamma}}{\sqrt{\gamma}} F_{\gamma_{D,2,x_2}}(\gamma) d\gamma$ , by using the same method to the CDF of  $x_1$  in (14b).

### 3.4. Throughput in Delay-Limited Transmission Mode

In fact, the throughput is examined by  $OP$  at a fixed transmission rate. For simplicity, we assume that the source transmits data at a fixed rate,  $R_0$  (bits/sec/Hz), and the  $OP$  is important to the throughput defined as  $R_0 = 2^{2\gamma_0} - 1$  (bps/Hz) with  $1/2$  being the effective communication time. Therefore, the throughput,  $\tau$  at  $D$  is written by

$$\tau_{D,x_1} = \frac{1}{2} R_0 (1 - OP_{x_1}), \quad (32a)$$

and

$$\tau_{D,x_2} = \frac{1}{2} R_0 (1 - OP_{x_2}). \quad (32b)$$



#### 4. Numerical Results

In this section, we prove the correctness of the system by providing simulation results. In addition, comparisons with Monte Carlo performance results are also given. It is noted that we generate  $10^6$  realizations of Rayleigh distribution. In addition, we assume  $S, R$  and  $D$  are collinear with  $R$  located between  $S$  and  $D$ . For simplicity of presentation, we summarize the used parameters in Table 1.

**Table 1.** Simulation parameters.

Symbols	Parameter Names	Values
$R_0$	Source rate	1 (bps/Hz)
$\rho$	PS ratio	0.2
$m$	Path-loss	2.7
$\eta$	Energy harvesting efficiency	0.8
$d_{SD}$	Distance of $S$ - $D$ link	1
$d_{SR}$	Distance of $S$ - $R$ link	0.3
$d_{RD}$	Distance $R$ - $D$ link	$d_{SD} - d_{SR}$
$\Omega_{f_1}$	Mean of the exponential RVs $ f_1 ^2$	1
$\Omega_{f_2}$	Mean of the exponential RVs $ f_2 ^2$	1
$\Omega_{f_3}$	Mean of the exponential RVs $ f_3 ^2$	1

In Figure 3, we compare  $OP$  with two defined thresholds in two cases, i.e., Case 1:  $\gamma_0 = 1$  and Case 2:  $\gamma_0 = 3$  (bps/Hz). It is clear that the lower the threshold is, the better  $OP$  becomes. In contrast, the  $OP$  falls when  $\beta$  climbs. In principle, when  $\beta$  rises, both  $S$  and  $R$  harvest more energy, so there is more energy for IT in the next hop. In this situation, the outage performance of  $x_1$  is superior to that of  $x_2$  due to the deployment of  $R$ .

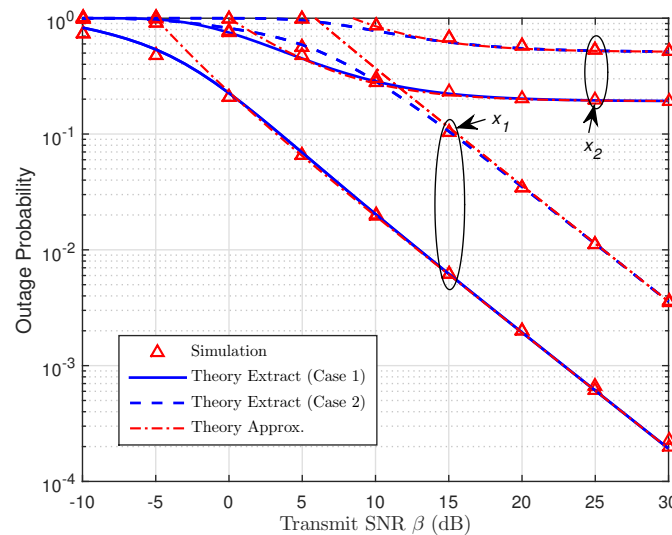


**Figure 3.** Outage probability ( $OP$ ) versus the transmit SNR,  $\beta$ .

In Figure 4, the throughput in the delay-limited transmission mode is presented as a function of  $\beta$  in the two cases regarding distances, including Case 1:  $d_{SR} = 0.2$  and Case 2:  $d_{SR} = 0.3$ . We can see that  $x_1$  enjoys better throughput due to its lowest  $OP$ , the short distance between  $S$  and  $R$ , and the higher amount of harvested energy. It also presents the throughput ceilings at high SNR regime because the  $OP$  increasingly approaches zero, and the throughput is determined by the pre-defined data rate. However, regarding  $x_2$ , the throughput is worse because of the lack of energy for information decoding, so outage events can occur which compromise the throughput performance. As a result,

the suitable placement of  $R$  in the design of practical CR-NOMA transmission systems is proved to be important.

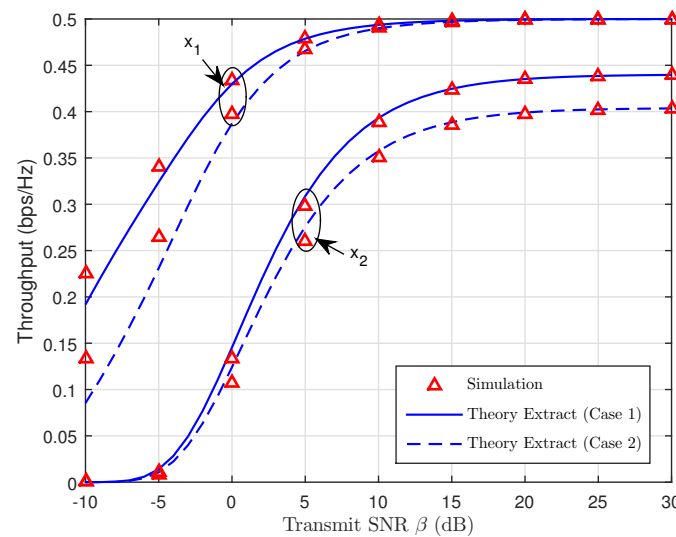


Figure 4. Throughput versus the transmit SNR,  $\beta$ .

As illustrated in Figure 5, the throughput performance of both CR-NOMA and traditional CR-OMA is depicted versus the PS ratio. It is noted that we set the transmit power,  $P_S$  to two fixed values of 0 (dB) and 5 (dB). It is clear that the throughput performance of CR-NOMA is significantly higher compared to CR-OMA, in which the performance gap becomes clear during the end of the period. This is because due to the deployment of SIC at  $D$  in the second time slot, the transmission of data symbol  $x_2$  becomes possible. In addition, thanks to the use of  $R$ , the distance between  $R$  and  $D$  can be effectively reduced to minimize the fading gain of  $x_1$ .

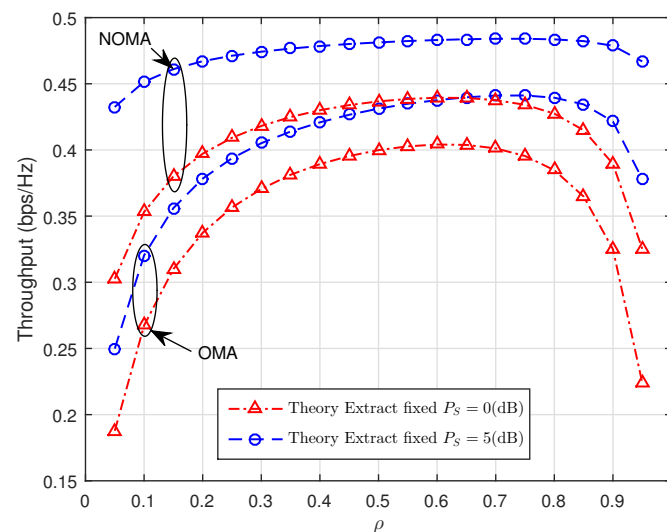


Figure 5. Throughput versus power splitting (PS) ratio,  $\rho$ .

In Figure 6, the ABEP is presented as a function of the transmit SNR,  $\beta$ . It is obvious that due to the high quality of the  $R$ - $D$  link, the ABEP for the data symbol  $x_1$  also improves. Nevertheless, the gap between the corresponding curves becomes noticeable as  $\rho$  climbs, especially with the data symbol  $x_2$ . Additionally, the ABEP of  $x_2$  is limited to the transmit power of the  $R$ - $D$  link.

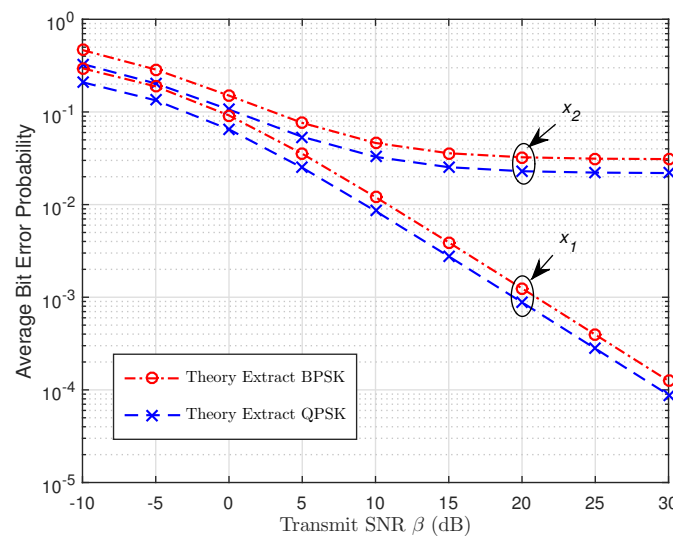


Figure 6. ABEP versus the transmit SNR,  $\beta$ .

As depicted in Figure 7, we present the transmission rate as a function of the transmit SNR,  $\beta$  when  $a_1 = 0.9$ ,  $a_2 = 0.1$ , and  $\Omega_{f_1} = \Omega_{f_2} = 10(\text{dB})$ , and  $\Omega_{f_3} = 1(\text{dB})$ . It is noted that we achieve the performance gaps from (11a) and (11b). In particular, the total achievable rate of  $x_1$  is considered as the achievable rate transmitted in the fixed DF relaying scheme and the one directed transmitted from  $S$  to  $D$ . It is clear that the achievable rate in our considered system is enhanced thanks to the deployment of PS WSN-NOMA protocol compared to the existing PS-OMA respectively discussed in [30] and CRS-NOMA in [31]. Unlike PS-OMA and CRS-NOMA which only have the relay transmitting the decoded symbol to the destination in the second time slot, our system deploys SIC technique in which  $S$  can transmit symbols to  $D$ , and  $D$  can use SIC technique to decode the data symbols.

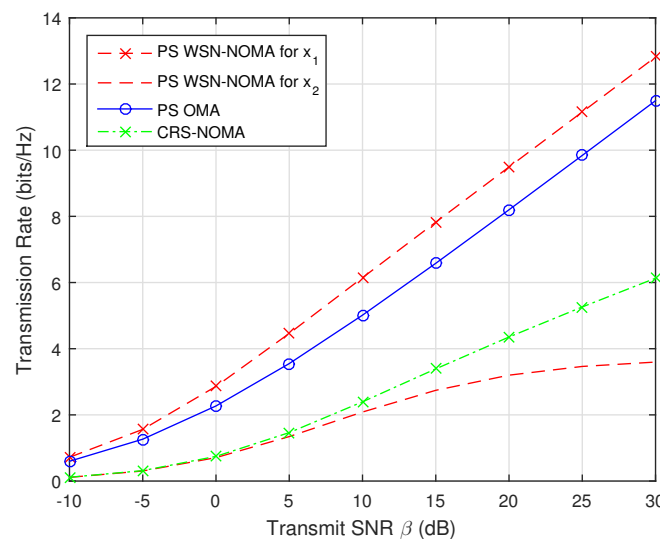


Figure 7. Transmission rate versus the transmit SNR,  $\beta$ .

## 5. Conclusions

In this paper, we studied a CR-NOMA network using PS receiver architecture. To analyze the system performance, we obtained closed-form exact and approximate expressions for OP. Following that, ABEP was examined, and the expression for delay-limited throughput was also derived. With the provided simulation results, better outage and throughput performance were witnessed.

**Author Contributions:** T.T.H.L. and H.-S.N. conceived the idea; H.-S.N. and V.V.H. designed the experiments, performed the simulation experiments and analyzed the data; H.-S.N. and T.-L.N. contributed to developing some mathematical analysis parts; T.-S.N. and T.-L.N. organized and wrote the paper; T.-S.N. and M.V. critically reviewed the organization of the paper.

**Acknowledgments:** This work was supported by the grant SGS reg. No. SP2019/41 conducted at VSB Technical University of Ostrava, Czech Republic and partly by The Ministry of Education, Youth and Sports from the Large Infrastructures for Research, Experimental Development, and Innovations project reg. no LM2015070.

**Conflicts of Interest:** The authors declare that they have no competing interests.

## Abbreviations

The following abbreviations are used in this manuscript:

NOMA	Non-orthogonal multiple access
SWIPT	Simultaneous wireless information and power transfer
WSN	wireless sensor network
EH	Energy harvesting
IT	Information transmission
SIC	Successive interference cancellation
PS	Power splitting
AF	Amplify-and-forward
DF	Decode-and-forward
OP	Outage probability
ABEP	Average bit error probability

## References

1. Sudevalayam, S.; Kulkarni, P. Energy Harvesting Sensor Nodes: Survey and Implication. *IEEE Commun. Surv. Tutor.* **2011**, *13*, 443–461. [\[CrossRef\]](#)
2. Tung, N.T. Heuristic Energy-Efficient Routing Solutions to Extend the Lifetime of Wireless Ad-Hoc Sensor Networks. In *Intelligent Information and Database Systems. ACIIDS 2012; Lecture Notes in Computer Science*; Springer: Berlin/Heidelberg, Germany, 2012; Volume 7197, pp. 487–497.
3. Tung, N.; Vinh, P. The Energy-Aware Operational Time of Wireless Ad-Hoc Sensor Networks. *Mob. Netw. Appl.* **2013**, *18*, 454–463. [\[CrossRef\]](#)
4. Lu, X.; Wang, P.; Niyato, D.; Kim, D.I.; Hann, Z. Wireless Networks with RF Energy Harvesting: A Contemporary Survey. *IEEE Commun. Surv. Tutor.* **2015**, *17*, 757–7891. [\[CrossRef\]](#)
5. Ku, M.L.; Li, W.; Chen, Y.; Liu, K.J.R. Advances in Energy Harvesting Communications: Past, Present, and Future Challenge. *IEEE Commun. Surv. Tutor.* **2016**, *18*, 1384–1412. [\[CrossRef\]](#)
6. Liu, K.; Zhu, Q.; Wang, Y. Allocation Optimization for Multiple Energy-Harvesting Relay System Using SWIPT. *Mob. Inf. Syst.* **2018**, *2018*, 7102427. [\[CrossRef\]](#)
7. Ni, Z.; Motani, M. Performance of Energy-Harvesting Receivers with Time-Switching Architecture. *IEEE Trans. Wirel. Commun.* **2017**, *16*, 7252–7263. [\[CrossRef\]](#)
8. Zhou, Z.; Peng, M.; Zhao, Z.; Li, Y. Joint Power Splitting and Antenna Selection in Energy Harvesting Relay Channels. *IEEE Signal Process. Lett.* **2015**, *16*, 7252–7263. [\[CrossRef\]](#)
9. Nguyen, H.S.; Nguyen, T.S.; Nguyen, M.T.; Voznak, M. Optimal Time Switching-Based Policies for Efficient Transmit Power in Wireless Energy Harvesting Small Cell Cognitive Relaying Networks. *Wirel. Pers. Commun.* **2015**, *99*, 1605–1624. [\[CrossRef\]](#)
10. Zhong, S.; Huang, H.; Li, R. Outage probability of power splitting SWIPT two-way relay networks in Nakagami-m fading. *EURASIP J. Wirel. Commun. Netw.* **2018**, *2018*, 11. [\[CrossRef\]](#)
11. Bai, X.; Shao, J.; Tian, J.; Shi, L. Power-Splitting Scheme for Nonlinear Energy Harvesting AF Relaying with Direct Link. *Wirel. Commun. Mob. Comput.* **2018**, *2018*, 7906957. [\[CrossRef\]](#)
12. Wang, T.; Lu, G.; Ye, Y.; Reni, Y. Dynamic Power Splitting Strategy for SWIPT Based Two-Way Multiplicative AF Relay Networks with Nonlinear Energy Harvesting Model. *Wirel. Commun. Mob. Comput.* **2018**, *2018*, 1802063. [\[CrossRef\]](#)

13. Kariminezhad, A.; Gherekhloo, S.; Sezgin, A. Optimal Power Splitting for Simultaneous Information Detection and Energy Harvesting. *IEEE Signal Process. Lett.* **2017**, *24*, 963–967. [[CrossRef](#)]
14. Liu, L.; Zhang, R.; Chua, K.C. Wireless Information and Power Transfer: A Dynamic Power Splitting Approach. *IEEE Trans. Commun.* **2013**, *61*, 3990–4001. [[CrossRef](#)]
15. Alsharoa, A.; Ghazzai, H.; Kamal, A.E.; Kadri, A. Optimization of a Power Splitting Protocol for Two-Way Multiple Energy Harvesting Relay System. *IEEE Trans. Green Commun. Netw.* **2017**, *1*, 444–457. [[CrossRef](#)]
16. Srivantana, T.; Maichalernnukul, K. Two-Way Multi-Antenna Relaying with Simultaneous Wireless Information and Power Transfer. *Symmetry* **2017**, *9*, 1–19. [[CrossRef](#)]
17. Wu, F.; Xiao, L.; Yang, D.; Cuthbert, L.; Liu, X. Transceiver Design and Power Allocation for SWIPT in MIMO Cognitive Radio Systems. *Symmetry* **2018**, *10*, 1–19. [[CrossRef](#)]
18. Dai, L.; Wang, B.; Ding, Z.; Wang, Z.; Chen, S.; Hanzo, L. A Survey of Non-Orthogonal Multiple Access for 5G. *IEEE Commun. Surv. Tutor.* **2018**, *20*, 2294–2323. [[CrossRef](#)]
19. Luo, S.; The, K.C. Adaptive Transmission for Cooperative NOMA System with Buffer-Aided Relaying. *IEEE Commun. Lett.* **2017**, *21*, 937–940. [[CrossRef](#)]
20. Alharbi, T.E.A.; So, D.K.C. Full-Duplex Decode-and-Forward Cooperative Non-Orthogonal Multiple Access. In Proceedings of the 2018 IEEE 87th Vehicular Technology Conference (VTC Spring), Porto, Portugal, 3–6 June 2018; pp. 2577–2465.
21. Zaidi, S.K.; Hasan, S.F.; Gui, X. Evaluating the Ergodic Rate in SWIPT-Aided Hybrid NOMA. *IEEE Commun. Lett.* **2018**, *22*, 1870–1873. [[CrossRef](#)]
22. Ashraf, M.; Shahid, A.; Jang, J.W.; Lee, K.G. Energy Harvesting Non-Orthogonal Multiple Access System with Multi-Antenna Relay and Base Station. *IEEE Access* **2017**, *5*, 17660–17670. [[CrossRef](#)]
23. Zhang, Y.; Ge, J. Performance analysis for non-orthogonal multiple access in energy harvesting relaying networks. *IET Commun.* **2016**, *11*, 1768–17740. [[CrossRef](#)]
24. Lv, L.; Chen, J.; Ni, Q.; Ding, Z.; Jiang, H. Cognitive Non-Orthogonal Multiple Access with Cooperative Relaying: A New Wireless Frontier for 5G Spectrum Sharing. *IEEE Commun. Mag.* **2018**, *56*, 188–195. [[CrossRef](#)]
25. Anwar, A.; Seet, B.C.; Din, Z. Non-Orthogonal Multiple Access for Ubiquitous Wireless Sensor Networks. *Sensors* **2018**, *18*, 516. [[CrossRef](#)] [[PubMed](#)]
26. Song, M.; Zhen, M. Energy Efficiency Optimization For Wireless Powered Sensor Networks with Nonorthogonal Multiple Access. *IEEE Sens. Lett.* **2018**, *2*, 2475–1472. [[CrossRef](#)]
27. Haci, H.; Zhu, H.; Wang, J. Performance of Non-orthogonal Multiple Access with a Novel Asynchronous Interference Cancellation Technique. *IEEE Trans. Commun.* **2017**, *65*, 1319–1335. [[CrossRef](#)]
28. Zwillinger, D. *Table of Integrals, Series, and Products*, 8th ed.; Elsevier: New York, NY, USA, 2014.
29. Cho, K.; Yoon, D. On the general BER expression of one and two dimensional amplitude modulations. *IEEE Trans. Commun.* **2002**, *50*, 1074–1080.
30. Nasir, A.A.; Zhou, X.; Durrani, S.; Kennedy, R.A. Throughput and ergodic capacity of wireless energy harvesting based DF relaying network. In Proceedings of the IEEE International Conference on Communications (ICC), Sydney, Australia, 10–14 June 2014; pp. 4066–4071.
31. Kim, J.B.; Lee, I.H. Capacity Analysis of Cooperative Relaying Systems Using Non-Orthogonal Multiple Access. *IEEE Commun. Lett.* **2015**, *19*, 1949–1952. [[CrossRef](#)]

